The HI Supergiant Shells in the Large Magellanic Cloud

S. Kim[1], L. Staveley-Smith[2], R.J. Sault[2], M.J. Kesteven[2], D. McConnell[2], M.A. Dopita[1], and M. Bessell[1]

[1] Mount Stromlo and Siding Spring Observatories, Weston Creek PO. ACT 2611, Australia
[2] Australia Telescope National Facility, CSIRO, 76 Epping, NSW 2121, Australia

Abstract. We present the result of an HI aperture synthesis mosaic of the Large Magellanic cloud (LMC), made recently with the Australia Telescope Compact Array (ATCA). The resolution of the mosaiced images is 1.'0 (15 pc, using a distance to the LMC of 50 kpc). In contrast to its appearance at other wavelengths, the LMC is remarkably symmetrical in HI on the largest scales, with the bulk of the HI residing in a disk of diameter 8.°4 (7.3 kpc). Outer spiral structure is clearly seen, though the features appear to be due to differential rotation, therefore transient in nature. On small to medium scales, the combined action of numerous shells and supershells dominate the structures and motions of the HI gas in the LMC. A good correlation is seen between supershells previously identified in Hα (e.g. Meaburn 1980) and HI structures. We compare the results with a new wide-field Hα image.

1 Introduction

We completed the high resolution HI survey of the Large Magellanic Cloud with the Australia Telescope Compact Array (ATCA). The LMC has been studied in neutral hydrogen gas with Parkes Telescope by McGee and Milton (1966), Rohlfs et al. (1984) and Luks and Rohlfs (1992), but the spatial resolution of these previous surveys was 14.9' (220 pc). The new survey with the ATCA has much higher spatial resolution, 1' (15 pc). We compare the HI distribution in the LMC to the distribution of Hα emission, taken with a camera lens mounted on the 16 inch at Mount Stromlo and Siding Spring Observatories. The Hα images cover the same area of HI Mosaic survey with a spatial resolution of 20". These two surveys offer a unique probe of the detailed relationship between the ionized phase and atomic phase in the gas of the LMC.

2 Observations and Data Reduction

The detailed observing strategy and the data reduction, which involves the mosaicing together of 1344 fields are described in Kim et al. (1997). The

https://doi.org/10.1017/S0252921100071542 Published online by Cambridge University Press

central observing frequency was 1.419 GHz, corresponding to a central heliocentric velocity of 297 km s^{-1} , a velocity coverage of -33 to 627 km s^{-1} with a velocity resolution of 1.65 km s^{-1} .

For the wide-field survey of Hα emission in the LMC, a Nikon 30.72 mm $f/5.0$ camera lens was mounted on the 16 inch Telescope with a filter assembly and a cooled (2048 × 2148) CCD. Each 15 μm pixel corresponds to 20."63 on the sky, giving a total field size of 11.7° square. The Hα filter was centered at 6569 $\AA$ with a FWHM of 15 $\AA$. Continuum subtraction was done with another image centered at 6620 $\AA$. The exposure time for both Hα and continuum images was 4 × 900 s.

3 Results

Figure 1 shows the HI brightness temperature map of the LMC, constructed from the brightest HI component at each spatial position. The coordinate scale is a J2000 tangent plane centered on $\alpha = 05^h23^m$, δ=-69°44'(J2000). The heliocentric velocity range in which we find HI emission is 190 - 370 km s^{-1} . On the large scales, the HI distribution in the LMC is nearly axisymmetric, in contrast with Hα emission from the result of a new Hα survey (Fig. 2). The geometric inclination obtained from the axial ratio (a/b) of the apparent ellipse is 22°.

In the channel maps, we see the southern spiral pattern which is close to the optical bar and extends out from the 'B3' stub, tentatively identified by de Vaucouleurs and Freeman (1972). This pattern appears in the velocity range, 215 - 258 km s^{-1} . In the velocity range, 202 - 289 km s^{-1} , the HI gas in the LMC has stretched toward the HI bridge between the LMC and the SMC.

On the smaller scales, the peak brightness temperature map of the LMC shows filamentary structures, combined with HI holes and shells. In our preliminary analysis we have defined 32 HI supergiant shells (Fig. 2). The selection criteria we applied are 1) The HI shells (edge-brightened ring-like structure), larger than 600 pc are visible in at least three integrated channel maps (the line width of each integrated channel map is 5 km s^{-1}), and 2) The approaching and receding hemispheres (or one of the hemispheres) are visible in position-velocity cuts (P-V) diagrams.

Many of the shells are difficult to identify as expanding shells in the P-V diagrams due to relatively low sensitivity resulting from the lack of HI inside shells and confusion of interlocking shells.

If we compare the distribution of HI Supergiant shells in each of the four quadrants of the LMC, we clearly see that the largest number of shells are located in the south-eastern quadrant, near the 30 Doradus nebula (Fig. 2). Fig. 2 also shows the age of each shell, t_s (in units of Myr), calculated from $t_s = (3/5)(R_s/V_s)$ given by the standard theory of wind-driven bubbles

https://doi.org/10.1017/S0252921100071542 Published online by Cambridge University Press

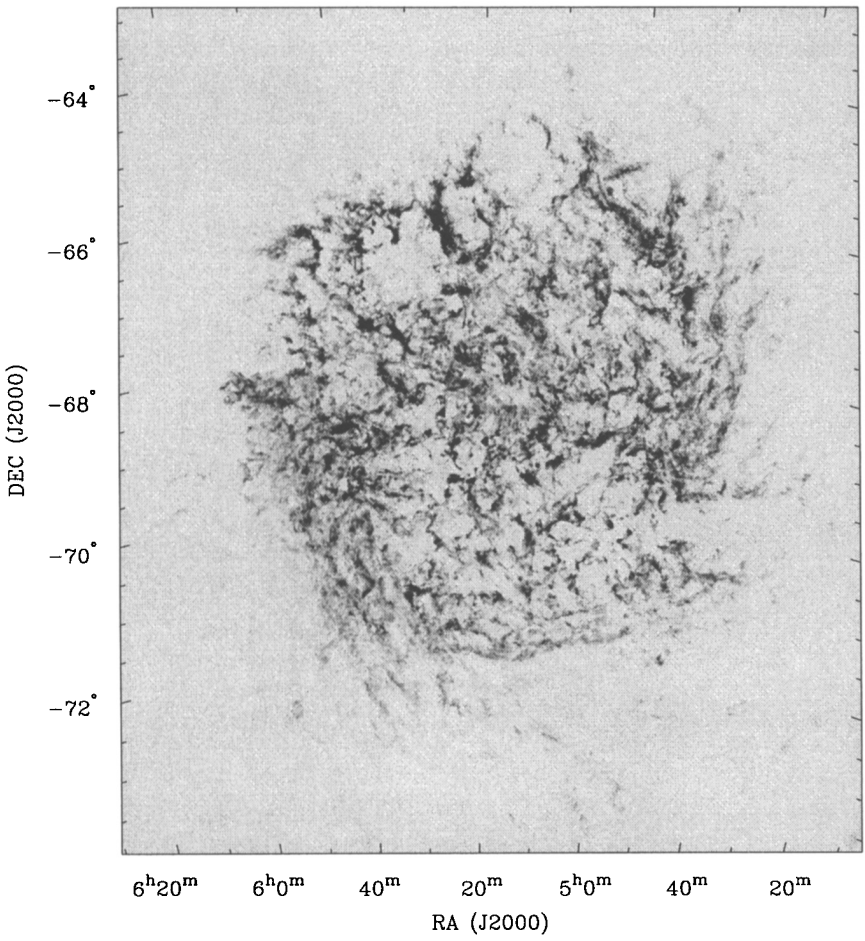

Fig. 1. The peak 21-cm brightness temperature map (measured at each channel) from the ATCA survey of HI in the LMC.

(Weaver et al. 1977). R_s is the shell radius in units of pc and V_s is the expansion velocity of the shell in units of $\mathrm{km\,s^{-1}}$.

The measured ages of these expanding supergiant shells are distributed between 3 Myr and 25 Myr. The bubbles in Fig. 2 may also be classified morphologically by comparing the HI and Hα structure. We define five categories for the geometrical correlation between HI and Hα emission. This should be approximately an age sequence. In Type I shells, the HI shells are filled with ionized gas or else include discrete HII regions inside the HI shell. In Type II shells the ionized gas forms a thin shell and has been trapped by the HI shell. Type III represents HI shells which have discrete HII regions on the wall of the shell. Type IV is an HI shell which is not associated with ionized

https://doi.org/10.1017/S0252921100071542 Published online by Cambridge University Press

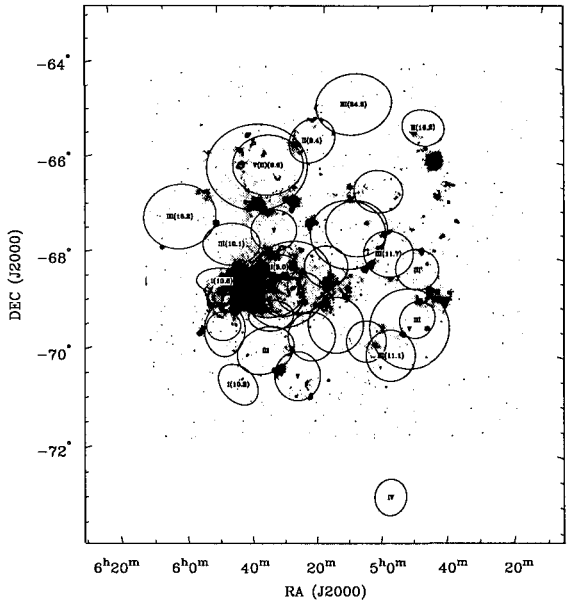

Fig. 2. The position of preliminarily defined HI supergiant shells are overlaid as ellipses on the Hα image from this survey. The classification, based on the comparison with HI shells and Hα is marked and the numbers indicate the age of the shells in Myrs.

gas. Type III and Type IV might have both evolved from Type II and the difference of two types is probably dependent on the density of the interstellar medium. Type V are HI shells which have morphologically complex structure, which might be caused by the triggered star formation due to the expanding shell. Shells near 30 Dor and some other regions are very confused and have not been classified. No age in some of the shells marked in Fig. 2 is due to these objects having very uncertain or unmeasurable expansion velocities.

References

de Vaucouleurs, G. and Freeman, K.C. (1972): Vistas in Astronomy 14, 163
Kim, S., Staveley-Smith, L., Sault, R.J., Kesteven, M. J., Mcconnell, D.(1997): A&A, to be submitted
Luks, T., & Rohlfs, K. (1992): A&A 263, 41
McGee, R.X., & Milton, J.A. (1966): Aust.J.Phys. 19, 343
Meaburn, J. (1980): MNRAS 192, 365
Rohlfs, K. et al.(1984): A&A 137, 343
Weaver, R., McCray, R., Castor, J., Shapiro, P., Moore, R. (1977): ApJ 218, 377

https://doi.org/10.1017/S0252921100071542 Published online by Cambridge University Press